ACS APPLIED MATERIALS & INTERFACES

www.acsami.org Research Article

High-Performance Thermomagnetic Gd−Si−Ge Alloys

Saurabh Singh,* Na Liu, Yu Zhang, Amin Nozariasbmarz,* Sumanta Kumar Karan, Lavanya Raman, Gagan Kumar Goyal, Shweta Sharma, Wenjie Li, Shashank Priya, and Bed Poudel*

Cite This: https://doi.org/10.1021/acsami.3c03158 Read Online

ACCESS | Metrics & More | Article Recommendations | Supporting Information

ABSTRACT: Exploring low-grade waste heat energy harvesting is crucial to address increasing environmental concerns. Thermomagnetic materials are magnetic phase change materials that enable energy harvesting from low-temperature gradients. To achieve a high thermomagnetic conversion efficiency, there are three main material requirements: (i) magnetic phase transition near room temperature, (ii) a substantial change in magnetization with temperature, and (iii) high thermal conductivity. Here, we demonstrate a high-performance $Gd_5Si_{2.4}Ge_{1.6}$ thermomagnetic alloy that meets these three requirements. The magnetic phase transition temperature was successfully shifted to 306 K by introducing Ge doping in Gd_5Si_4, and a sharper and more symmetric magnetization behavior with saturation magnetization of M_{max} = 70 emu/g at a 2 T magnetic field was achieved in the ferromagnetic state. The addition of SeS_2, as a low-temperature sintering aid, to the Gd−Si−Ge alloy improved the material's density and thermal conductivity by ∼45 and ∼275%, respectively. Our results confirm that the $(Gd_5Si_{2.4}Ge_{1.6})_{0.9}(SeS_2)_{0.1}$ alloy is a suitable composite material for low-grade waste heat recovery in thermomagnetic applications.

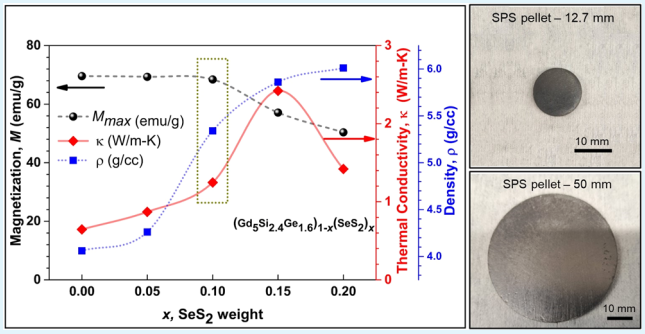

KEYWORDS: *thermomagnetic, phase transition, low-grade thermal energy harvesting, magnetic alloys, gadolinium*

■ INTRODUCTION

Low-grade waste heat harvesting is appealing as ∼63% of overall energy is dissipated in the form of low-grade waste heat (hot-side temperature below 100 °C).[1−7] Thermomagnetic (TM) generators are a promising method for low-grade waste heat recovery and will have a wide range of practical applications in electronic sensors and devices.[8−11] Near Curie temperature (T_c), the temperature at which a TM material (TMM) changes from the ferromagnetic (FM) state to paramagnetic (PM) state and vice versa, TMMs possess large magnetization (M_{cold}), which turns into a low magnetization value (M_{hot}) above T_c.[12,13] In a complete TM cycle, a device can harvest the magnetic energy, defined as $E_m = +\mu_0 \Delta MH$, where μ_0 and H are the magnetic field constant and applied external magnetic field, respectively.[14] The material's efficiency for the conversion of thermal input energy (Q_{in}) into useful output energy via thermomagnetic material is defined as $\eta = \frac{E_m}{Q_{in}} = \frac{\mu_0 \Delta MH}{Q_{in}}$. From the expression of energy and efficiency, it is noticeable that a large change in the magnetic moment, i.e., $\Delta M = M_{cold} - M_{hot}$, in a small temperature difference ($\Delta T = T_{hot} - T_{cold}$) is a key material property for an efficient TM device.[8] A TMM showing reversible and second-order phase transition would be a suitable choice for the minimum energy loss during the TM cycle. A large value of power density (P_D), defined as $P_D = E_m \cdot f$, harvested by TM devices is achieved by increasing the magnetic energy (E_m) and cycle frequency (f). This condition demands a large change in the magnetic moment together with high thermal conductivity (κ) for efficient and quick heat exchange in the vicinity of the ΔT across its magnetic phase transition.[8]

In the past several years, different types of materials including transition metals (Fe, Co, Ni), rare earth elements (Gd, Tb),[15] intermetallic compounds (La−Fe−Co−Si-based),[15,16] metallic antiperovskites ($Sn_{0.2}Ga_{0.8}CFe_3$, $Ga_{0.92}CMn_{3.08}$),[17,18] oxide perovskites ($La_{0.67}Ba_{0.33}MnO_3$, $La_{0.7}Nd_{0.1}Na_{0.2}MnO_3$),[19,20] and amorphous glasses ($Gd_{48}Co_{52}$) have been investigated due to their potential for TM applications.[21,22] Among these, gadolinium (Gd) fulfills the fundamental requirements to be used as a TMM near room temperature.[23−25] With a reasonable change in the magnetic moment ($\Delta M \sim 77$ emu/g with $\Delta T = 30$ K), moderate κ (6.6 W m^{-1} K^{-1}), and $T_C \sim 293$ K, Gd has been widely explored,[26] and its device performance has been investigated using numerical modeling and experimental techniques.[27−33] Considering the value of T_C, pure Gd requires additional cooling

Received: March 4, 2023
Accepted: June 29, 2023

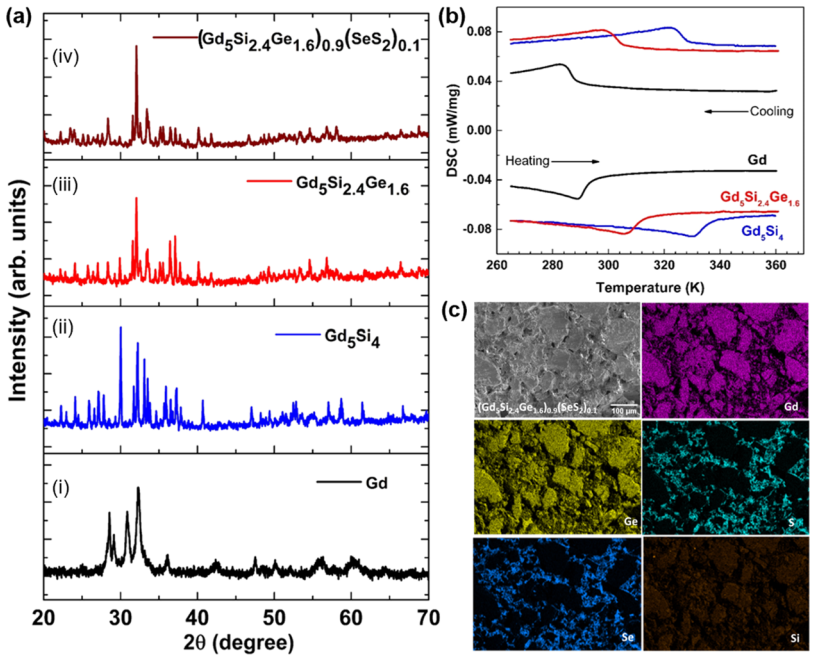

Figure 1. (a) XRD patterns of as-synthesized powder samples of (i) Gd, (ii) Gd_5Si_4, (iii) $Gd_5Si_{2.4}Ge_{1.6}$, and (iv) $(Gd_5Si_{2.4}Ge_{1.6})_{0.9}$ $(SeS_2)_{0.1}$. (b) Differential scanning calorimetry (DSC) curves for Gd, Gd_5Si_4, $Gd_5Si_{2.4}Ge_{1.6}$, and $(Gd_5Si_{2.4}Ge_{1.6})_{0.9}(SeS_2)_{0.1}$ compounds. (c) SEM and EDS images of $(Gd_5Si_{2.4}Ge_{1.6})_{0.9}(SeS_2)_{0.1}$ showing the distribution of Se and S in the microstructure.

below 300 K, which makes the device design complex. In addition, Gd is brittle and forms gadolinium hydroxide in contact with cold/hot water, which degrades its mechanical, thermal, and magnetic properties.[8,58,59] Several Gd-based materials have been investigated by alloying with silicon and/or germanium.[34−38] The alloying of Si/Ge with Gd to form a GdSi−GdGe pseudobinary system allows the tuning of magnetic phase transition T_C in a wide temperature range of 40−340 K.[39] Besides the allowed freedom of tunable magnetic properties, GdSi−GdGe pseudobinary systems make these materials prominent for magnetocaloric/thermomagnetic properties; however, studies on the densification of these alloys are lacking due to the brittle nature of this material that prevents it from making the shape of cylinder or plate. Also, an investigation of thermal properties is needed to determine the bulk size of materials to know the applicability of these alloys for thermomagnetic applications. In addition to the silicon and germanium doping in Gd, making alloys of Gd with transition metals (Mn, Zn, Ni, Pd) and rare earth elements (Nd and Pr) has been found useful in the improvement of the thermal and magnetic properties favorable for the magnetocaloric applications.[40−43] It is worth mentioning here that in the field of magnetocaloric effect, Gd−Si−Ge alloys have been widely investigated to find their potential applicability for magnetic refrigeration applications, mainly below room temperature. In this direction, Gębara et al. systematically investigated the nature of phase transition of GdGeSi-(X)-type alloys (where x = Ni, Nd, and Pr) using heat and magnetic transport techniques.[43,44] The alloys $Gd_{80}Ge_{15}Si_5$ and $Gd_{75}Ge_{15}Si_5Ni_5$ have the structural phase transition, which is confirmed as a first-order phase transition and shows a large magnitude of change in magnetic entropy ($\Delta S_M \sim 12$ J/kg·K). From the application perspective, such a large ΔS_M is good for magnetic refrigeration. In the case of $Gd_{75}Ge_{15}Si_5Pr_5$ and $Gd_{75}Ge_{15}Si_5Nd_5$, the nature of phase transition was noticed as second order, with a lower value of $\Delta S_M = \sim 5$ J/kg·K. Besides the good magnetocaloric effect shown by Gd−Ge−Si-X alloys, the phase transition temperature of all of these compounds is reported at much below the room temperature (300 K). On the other hand, in our daily lifestyle, plenty of low-grade waste heat energy is available in the temperature range of 300−320 K, which can be effectively harvested by Gd−Si−Ge-based alloys by utilizing the thermomagnetic effect.[8] For this application, the material's magnetic phase transition temperature should lie within the same temperature region, and finding the best composition of material with such magnetic properties is highly desirable. Motivated by this idea, the tuning of the magnetic phase transition temperature of Gd−Si−Ge materials in a temperature range of 300−320 K is studied in the present work.

A comprehensive investigation of the thermal transport and magnetic properties of Gd−Si−Ge-based materials with T_C values near room temperature is lacking. In addition, low-temperature densification and sintering methods are needed that do not cause deterioration of magnetic, mechanical, and thermal properties. For the materials sintered at high temperatures, there are chances of decomposition, precipitation, and structural phase change that will affect the magnetic properties. To overcome these problems, an engineered Gd-based alloy with tuned T_C between 300 and 310 K, higher ΔM, improved κ, and better mechanical properties is needed.[7,8,12]

Here, we systematically study the effect of selenium disulfide (SeS_2), as a new low-temperature sintering aid to substantially improve the TM properties of Gd−Si−Ge-based alloys near room temperature. We fabricated Gd_5Si_4 and $Gd_5Si_{2.4}Ge_{1.6}$ compounds through induction melting and densified the alloy by optimizing the SeS_2 percentage to improve the thermal conductivity by 90% while preserving the large magnetization. The physical property characterization confirms that the synthesized alloy is appropriate for TM applications at room temperature.

https://doi.org/10.1021/acsami.3c03158
ACS Appl. Mater. Interfaces XXXX, XXX, XXX−XXX

EXPERIMENTAL PROCEDURE

The chunks of Gd (99.9%, MSE supplies), Si (99.9999%, Alfa Aesar), and Ge (99.999%, Thermo Fisher Scientific) were weighed in a stoichiometric proportion for the synthesis of Gd_5Si_4 and $Gd_5Si_{2.4}Ge_{1.6}$ compounds. The raw materials were melted by induction melting in a boron nitride crucible under an argon atmosphere (gas flow pressure 30 Pa). The as-melted ingot was cylindrical with a dimension of ∼20 mm diameter and ∼5 mm height. The ingot was pulverized into a fine powder by hand grinding (∼20 min) using a mortar and pestle. The different weight percentages of SeS_2 (97%, Alfa Aesar), as a low-temperature sintering agent, were mixed homogeneously with $Gd_5Si_{2.4}Ge_{1.6}$ alloys. The compositions are designated as $(Gd_5Si_{2.4}Ge_{1.6})_{1-x}(SeS_2)_x$, where x = 0.05, 0.10, 0.15, and 0.20. The powders were then consolidated in a cylindrical graphite die with an inner diameter of 12.7 mm using the spark plasma sintering (SPS) technique. The sintering temperature was 200 °C (heating rate with 1 °C/min) under a constant 40 MPa pressure for 2 min of soaking time. Further, the power of SPS was switched to obtain the sintered pellet at room temperature with a natural cooling condition. The TM pellets with a 12.7 mm diameter, a 50 mm diameter size, and an ∼2 mm height were prepared for thermal and magnetic property measurements.

Crystal structure and phase identification were studied on the powder sample by X-ray diffraction (XRD) technique using a PANalytical Empyrean (X-ray tube with Cu K_α source, wavelength 1.54 Å, voltage: 45 kV, current: 40 mA). The microstructure and elemental mapping were analyzed by a field emission scanning electron microscope (FESEM, FEI Verios), equipped with energy-dispersive X-ray spectroscopy (EDS, Oxford Aztec). The energy of the electron beam was set to 10 keV for the SEM mapping. The density (ρ) of the samples was measured using the Archimedes principle. Curie temperature (T_C), specific heat capacity (C_p), and heat flow were investigated using differential scanning calorimetry (DSC, 214 polyma NETZSCH) with a heating and cooling rate of 15 K/min. Temperature-dependent thermal diffusivity (D) of the samples was measured by using a Laser Flash instrument (LFA-467 HT HyperFlash). The thermal conductivity (κ) of the samples was then calculated from the relationship $\kappa = \rho \cdot C_p \cdot D$. Temperature-dependent magnetic measurements in the range of 300−350 K were performed using a vibrating sample magnetometer (VSM, Lakeshore 8600).

RESULTS AND DISCUSSION

The room-temperature XRD patterns of fine powders of each composition in comparison to those of Gd are shown in Figure 1a. For the Gd_5Si_4 sample, all of the XRD peaks correspond to the *orthorhombic I* crystal structure of Gd_5Si_4, classified by the same crystal symmetry and space group as *Pnma* (space group number 62, Pearson symbol *oP36*).[39,45] With the doping of Ge at the Si site in the Gd_5Si_4 system (Figure 1a), $Gd_5Si_{2.4}Ge_{1.6}$ possesses the same crystallographic phase as found for the Gd_5Si_4 structure. In the $Gd_5Si_{2.4}Ge_{1.6}$ sample, all XRD peaks are consistent with the data reported in the literature.[45] No structural phase change is noticed with the addition of SeS_2 into $Gd_5Si_{2.4}Ge_{1.6}$. The only difference is in the intensity ratio of peaks, mainly in the 2θ range of 25−45° (Figure 1a). The XRD data of Gd consist of Bragg reflection peaks, which correspond to the hexagonal closed pack (*hcp*) structure, classified by the space group *P*63/*mmc*, No. 194, and match well with the earlier report.[46]

Figure 1b shows the heat flow measurement as a function of temperature obtained from DSC measurement for Gd, Gd_5Si_4, $Gd_5Si_{2.4}Ge_{1.6}$, and $(Gd_5Si_{2.4}Ge_{1.6})_{0.9}(SeS_2)_{0.1}$ compounds. Si addition shifts T_C of Gd-based TMMs toward higher temperatures, and Ge is found to move the transition toward lower temperatures. The T_C of Gd, Gd_5Si_4, and $Gd_5Si_{2.4}Ge_{1.6}$ compounds are ∼290, 330, and 306 K, respectively. The phase transition temperature of Gd and Gd_5Si_4 is consistent with the earlier report.[39] In $Gd_5Si_{2.4}Ge_{1.6}$, the DSC shows a drastic decrement in the phase transition temperature. The phase diagram of Gd_5Si_4−Gd_5Ge_4 suggests that Gd_5Si_4 and $Gd_5Si_{2.4}Ge_{1.6}$ preserve the orthorhombic crystal structure,[39] and the earlier reports indicate that there is no change in the crystal structure across the phase transition temperature of Gd_5Si_4 and $Gd_5Si_{2.4}Ge_{1.6}$ compositions.[39] Gd forms an *hcp* structure at ambient pressure, and any change in the crystal structure occurs with applied external pressure.[42] In the present investigation, all of the compounds have been studied under ambient pressure. Therefore, the phase transition for all compounds can be attributed to the magnetic phase transition.

The observation of a step-down change in the DSC heating curve due to the magnetic phase transitions is similar to the structural phase transition driven by thermodynamic phase changes.[45−47] Likewise, a step-up change can be observed in the DSC cooling curve (Figure 1). In the cooling cycle, the phase transition temperatures of Gd, Gd_5Si_4, and $Gd_5Si_{2.4}Ge_{1.6}$ are shifted to ∼283, ∼ 322, and ∼298 K, respectively. The shift in transition temperature toward lower temperature is mainly due to the effect of the heating−cooling rate applied to the dynamical thermal phase investigation using DSC measurement.

An epoxy binder agent has been widely used as a sintering aid for brittle ceramic materials owing to its excellent adhesive nature.[48,49] However, due to its nonmagnetic properties, low density, and low κ, it is not a preferred choice for TM applications. This is mainly because of the formation of a nonhomogeneous thick layer of epoxy resin with lower density between the grains of TMMs. Such layers act as a scattering barrier for phonons and prevent heat flow propagation in the materials via grain-to-grain heat transfer. Owing to the large variations in mass density and difference in phonon mean free path of the activated phonon wave packets of epoxy materials and inorganic TMMs, the scattering probability of phonon wave packets (including low-mid and high range of frequencies) increases. Here, we demonstrate SeS_2 as an appropriate low-temperature sintering aid for improving the density and κ of TMMs. SEM image and EDS analysis of $(Gd_5Si_{2.4}Ge_{1.6})_{0.9}(SeS_2)_{0.1}$ show a uniform distribution of Gd, Si, and Ge elements, whereas the spaces between TMM grains are Se- and S-rich (Figures 1c and S1). SeS_2 binder distributes throughout the alloy and fills the area between the grains.

The low-temperature consolidation of $Gd_5Si_{2.4}Ge_{1.6}$ was performed at 200 °C using spark plasma sintering (SPS) for 2 min. SeS_2 plays a key role as a sintering aid for binding $Gd_5Si_{2.4}Ge_{1.6}$ particles to each other. Such low-temperature sintering prohibits phase change, grain growth, and precipitation in TMMs and maintains the magnetic properties as the magnetic domain structure within each grain is not affected at 200 °C.

In order to demonstrate a TM device, the synthesized powders need to be sintered to an appropriate desired shape. Initially, we tried to densify pure $Gd_5Si_{2.4}Ge_{1.6}$ through SPS; however, even at temperatures above 1000 °C, it did not sinter into a uniform dense sample, and more importantly, the magnetic properties dropped. The sintered sample was full of microcracks, and the alloy was unstable at room temperature. The sintering agent, SeS_2, with a density of 3 g/cm^3 and a melting point of 111 °C, was next used to densify the powders into a pellet. Figure 2 demonstrates the effect of the SeS_2

https://doi.org/10.1021/acsami.3c03158
ACS Appl. Mater. Interfaces XXXX, XXX, XXX−XXX

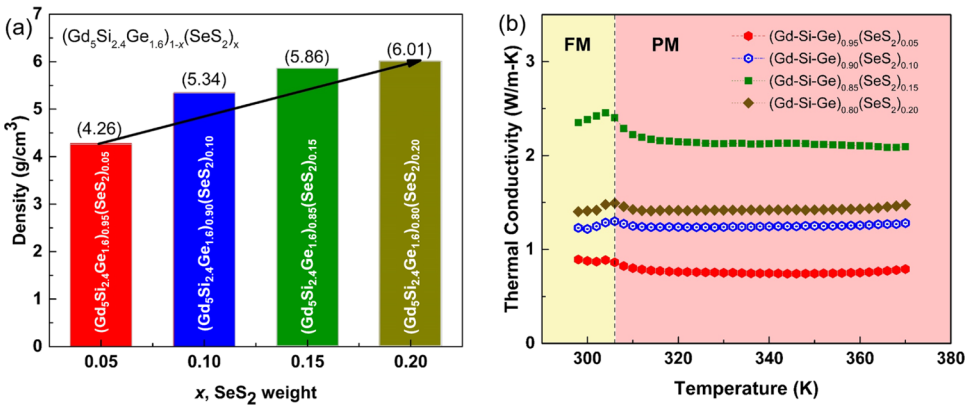

Figure 2. (a) Density evolution and (b) temperature-dependent thermal conductivity of $Gd_5Si_{2.4}Ge_{1.6}$ materials as a function of the SeS_2 weight ratio.

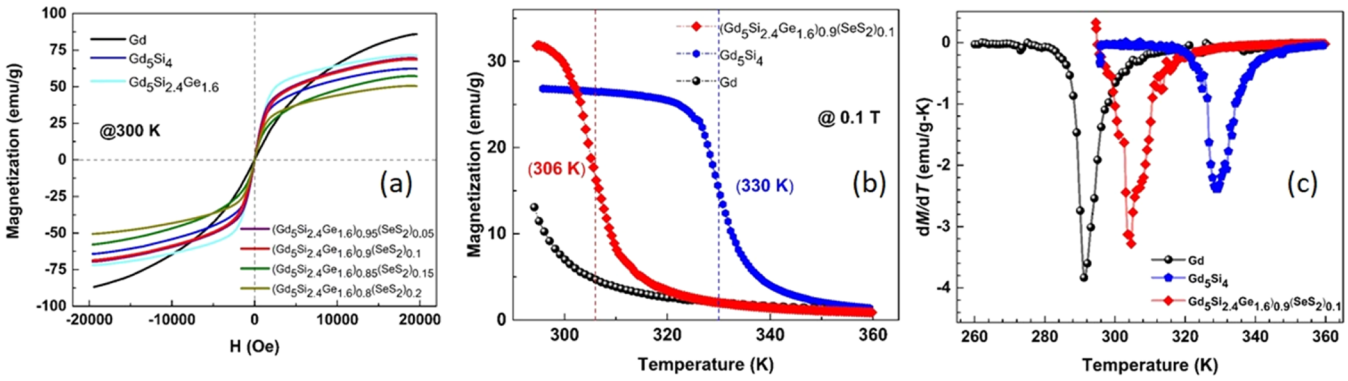

Figure 3. (a) Magnetization plot for induction melt ingots of Gd, Gd_5si_4, $Gd_5Si_{2.4}Ge_{1.6}$, and SPS samples $(Gd_5Si_{2.4}Ge_{1.6})_{1-x}(SeS_2)_x$ (x = 0.05, 0.1, 0.15, and 0.2) measured at 300 K. (b) Magnetization versus applied field measured at 300 K, (c) magnetization versus temperature measured at 0.1 T field, and (d) the rate of change of magnetization versus temperature.

concentration on the density and thermal conductivity of the $Gd_5Si_{2.4}Ge_{1.6}$ alloy. The density of all compositions increases monotonically with an increase in the SeS_2 concentration. The density of the $Gd_5Si_{2.4}Ge_{1.6}$ alloy with epoxy (prepared as a reference sample) reaches a maximum of 4.06 g/cm^3, which is the lowest value compared to that of SeS_2-contained alloys. Although the prepared ingot of $Gd_4Si_{2.6}Ge_{1.4}$ obtained from induction melting is in a cylindrical shape (shown in Figure S5a) and appears to be a solid shape, several cracks are formed and it gets brittle while cutting into the desired shape for further measurement. The measured density of a chunky piece of $Gd_5Si_{2.4}Ge_{1.6}$ is 4.13 g/cm^3. The densities of $(Gd_5Si_{2.4}Ge_{1.6})_{0.95}(SeS_2)_{0.05}$, $(Gd_5Si_{2.4}Ge_{1.6})_{0.9}(SeS_2)_{0.1}$, $(Gd_5Si_{2.4}Ge_{1.6})_{0.85}(SeS_2)_{0.15}$, and $(Gd_5Si_{2.4}Ge_{1.6})_{0.8}(SeS_2)_{0.2}$ are found to be 4.26, 5.34, 5.86, and 6.01 g/cm^3, respectively. Such an improvement in density is due to the adhesive nature of SeS_2 with a melting point of 111 °C, which fills the pores.

The measured values of specific heat and thermal diffusivity are shown in Figure S2a,b, respectively, in the Supporting Information. Temperature-dependent specific heat (C_p) of all compositions shows a kink near the phase transition temperature (Figure S2b). During the magnetic phase transition, the rearrangement of the spins inside the magnetic domain affects the magnon−phonon interactions within the domain, as well as at the grain boundaries. In the PM regime, there is a weak variation in the C_p, which might be due to the thermal agitation effect on randomly oriented spins within the magnetic domain as well as between the different neighboring domains. The thermal conductivity is improved by adding SeS_2 in the Gd−Si−Ge alloy due to a simultaneous increase in density and thermal diffusivity. The thermal conductivity increases around the phase transition temperature, while variation in the thermal conductivity of the FM phase ($T < T_c$ = 306 K) and the PM phase ($T > T_c$) as a function of temperature is negligible. This is advantageous for the fast heat exchange between the material and the working environment. This tendency toward heat flow behavior suggests that magnetic phase transition has a very weak effect on the phonon propagation through the magnon−phonon coupling once a stable magnetic phase region is achieved. In the high-temperature regime, magnetic ordering breaks down, and the PM phase does not affect the scattering probability of the phonon wave packets. In this strong scattering limit, the phonon mean free path does not get much affected and results in carrying almost the same heat flow.

The phase transition in TMMs is due to the change in magnetic ordering; therefore, the change in thermal conductivity across the phase transition region is broader and has a small variation in its magnitude. Structural phase change such as magnetic phase transition is a time-dependent phase transition and requires a specific amount of time for ordering and disordering, which results in a comparatively large variation in thermal diffusivity near phase transition.[50−52] The maximum thermal conductivity in the FM phase is found to be ∼2.15 W/m·K in the case of the $(Gd_5Si_{2.4}Ge_{1.6})_{0.85}(SeS_2)_{0.15}$ alloy, shown in Figure S3 in the

https://doi.org/10.1021/acsami.3c03158
ACS Appl. Mater. Interfaces XXXX, XXX, XXX−XXX

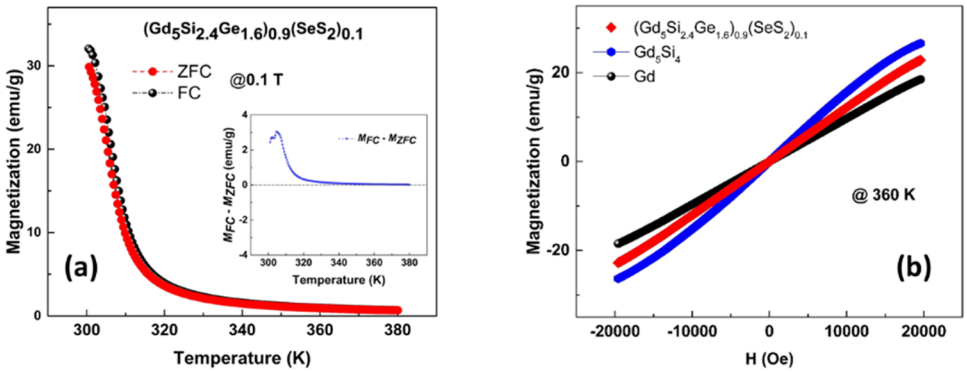

Figure 4. (a) Zero-field-cooled (ZFC) and field-cooled (FC) magnetization data with temperature for $(Gd_5Si_{2.4}Ge_{1.6})_{0.9}$ $(SeS_2)_{0.1}$ and (b) magnetization data measured at 360 K.

Supporting Information. The increasing trend in the magnitude of the thermal conductivity is observed up to the composition of $(Gd_5Si_{2.4}Ge_{1.6})_{0.85}(SeS_2)_{0.15}$ (i.e., $x > 0.15$). A further increase in the SeS_2 concentration results in a decrease in the magnitude of thermal diffusivity. Such behavior might be due to the optimum limit of the SeS_2 concentration in $Gd_5Si_{2.4}Ge_{1.6}$ for achieving the maximum heat diffusion. Above the threshold amount of SeS_2 ($x > 0.15$), the sintering aid suppresses the heat flow, even though the density of $(Gd_5Si_{2.4}Ge_{1.6})_{0.8}(SeS_2)_{0.2}$ is enhanced. A large improvement in the magnitude of κ is very useful for increasing the frequency of the thermal cycle of TMMs at the device level.[53−55]

The isothermal magnetization (M−H) plot for the induction melt $Gd_5Si_{2.4}Ge_{1.6}$ ingot and $(Gd_5Si_{2.4}Ge_{1.6})_{1-x}(SeS_2)_x$ (x = 0.05, 0.1, 0.15, and 0.2) measured at 300 K in comparison with Gd and Gd_5Si_4 is shown in Figure 3a. All samples show FM behavior with negligible coercivity. The M−H behavior suggests that the materials have almost zero energy loss during the TM cycle, and the M−H has a sharp slope around the zero magnetic field and reaches the saturation magnetization (M_s) value with an applied field strength of ∼2 T. The as-melt $Gd_5Si_{2.4}Ge_{1.6}$ has the highest M_s value of ∼71 emu/g. The value of M_s decreases when the as-melt sample is mixed with SeS_2. This is due to the additional nonmagnetic content in the matrix of TMM, which occupies a fraction of the magnetic material.

Although the addition of SeS_2 downgrades the saturation magnetization of the $Gd_5Si_{2.4}Ge_{1.6}$ alloy, the shape of the M−H curve and the negligible coercivity remain the same for all SeS_2-contained samples. This feature reveals that the non-magnetic SeS_2 does not change the magnetic nature of the $Gd_5Si_{2.4}Ge_{1.6}$ alloy rather than a small effect on the saturation magnetization. As shown in Figure 3a, the shape of the magnetization curve is sharper for Gd_5Si_4 and $(Gd_5Si_{2.4}Ge_{1.6})_{0.9}(SeS_2)_{0.1}$ as compared to the pure Gd material. This feature of M−H behavior results in a large magnetic energy (E_m) at a temperature just below the phase transition. The saturation magnetization of $(Gd_5Si_{2.4}Ge_{1.6})_{0.9}(SeS_2)_{0.1}$ is found to be higher in comparison to that of Gd_5Si_4 measured at the same temperature. Considering the physical, thermal, and magnetic properties of all samples, $(Gd_5Si_{2.4}Ge_{1.6})_{0.9}(SeS_2)_{0.1}$ shows the most optimum thermomagnetic properties compared to those of Gd, Gd_5Si_4, and $Gd_5Si_{2.4}Ge_{1.6}$.

Figure 3b shows the magnetization as a function of temperature at an applied magnetic field of 0.1 T (=1000 Oe) for Gd, Gd_5Si_4, and $(Gd_5Si_{2.4}Ge_{1.6})_{0.9}(SeS_2)_{0.1}$ in the temperature range of 293−360 K. For Gd_5Si_4 and $(Gd_5Si_{2.4}Ge_{1.6})_{0.9}(SeS_2)_{0.1}$, the magnetic phase transition region is clearly above room temperature, while pure Gd has a lower magnetic phase transition than room temperature. The addition of Si to Gd increases the T_C to 330 K, and Ge can compensate for the T_C to lower temperatures. This strategy is found to be more effective in tuning the T_c value within a 300−320 K temperature range, whereas the doping of transition metal or rare earth elements in Gd−Si−Ge suppresses the T_c values in 200−290 K, which is far below the room temperature.[40] The magnetic phase transition temperature for $(Gd_5Si_{2.4}Ge_{1.6})_{0.9}(SeS_2)_{0.1}$ shifts to 306 K, which makes this compound attractive for low-grade waste heat recovery near room temperature. This phase transition temperature is consistent with that observed from the DSC plot (Figure 1b). At higher-temperature regions (>360 K), the values of magnetization of all samples drastically reduce to M < 1 emu/g. Other important observations include the sharper and larger change in magnetization around T_C for the $(Gd_5Si_{2.4}Ge_{1.6})_{0.9}(SeS_2)_{0.1}$ alloy.

In the $(Gd_5Si_{2.4}Ge_{1.6})_{0.9}(SeS_2)_{0.1}$ alloy, the change in magnetization (ΔM) across its phase transition temperature is larger as compared to Gd_5Si_4, whereas its magnitude is slightly smaller than that of Gd when measured at a magnetic field of 0.1 T. This can also be confirmed by the dM/dT versus T plot as shown in Figure 3c. It can be observed from Figure 3b that $(Gd_5Si_{2.4}Ge_{1.6})_{0.9}(SeS_2)_{0.1}$ has a T_C of ∼ 306 K. Having a T_C value closer to room temperature makes $(Gd_5Si_{2.4}Ge_{1.6})_{0.9}(SeS_2)_{0.1}$ more suitable for TM application in comparison to the Gd with a T_C of ∼ 293 K much below room temperature. The value of ΔM ($M_{FM} - M_{PM}$) at a magnetic field of 0.1 T for $(Gd_5Si_{2.4}Ge_{1.6})_{0.9}(SeS_2)_{0.1}$ and Gd_5Si_4 is equal to ∼30 and ∼24 emu/g, respectively. The improvement in ΔM for $(Gd_5Si_{2.4}Ge_{1.6})_{0.9}(SeS_2)_{0.1}$ is ∼25% as compared to that for Gd_5Si_4. Such a large ΔM observed in the Gd−Si−Ge-based material near room temperature is a remarkable improvement in the magnetic properties within the Gd-based TM alloys. As shown in a comparative plot of magnetization in both FM and PM phases of $(Gd_5Si_{2.4}Ge_{1.6})_{1-x}(SeS_2)_x$ (x = 0.05, 0.1, 0.15, and 0.2) (Figure S4, Supporting Information), the magnetization values are decreased after x = 0.1 in the base composition. This suggests that $(Gd_5Si_{2.4}Ge_{1.6})_{0.9}(SeS_2)_{0.1}$ provides good magnetic properties as compared to those of the alloys without SeS_2.

In order to investigate the nature of magnetic behavior in the vicinity of the magnetic phase transition temperature, we have performed zero-field cooling (ZFC) and field cooling (FC)

https://doi.org/10.1021/acsami.3c03158
ACS Appl. Mater. Interfaces XXXX, XXX, XXX−XXX

magnetization measurements of the $(Gd_5Si_{2.4}Ge_{1.6})_{0.9}(SeS_2)_{0.1}$ alloy at 0.1 T in the temperature range of 300−360 K as shown in Figure 4a. In the PM phase regime, both ZFC and FC data overlap each other above 320 K. In the PM region, the magnetic moment within the domain is expected in the disordered configuration due to the thermal agitation and therefore has no difference in ZFC and FC data. However, there is a significant difference in ZFC and FC data below 320 K, and this difference increases to ∼3 emu/g when the material reaches the state of the FM phase. This suggests that $(Gd_5Si_{2.4}Ge_{1.6})_{0.9}(SeS_2)_{0.1}$ has intrinsic magnetic characteristics and goes through the PM-to-FM transition when it is cooled below the Curie temperature. Also, the $M-H$ curve for the PM phase measured at high temperatures, as shown in Figure 4b, confirms the PM nature of all three samples by showing an almost linear behavior.

For a good TM material, large changes in the magnetic moment and Curie temperature are the most important and primary decisive physical quantities, whereas κ and ρ are secondary. Figure 5 shows a comparative plot of three main

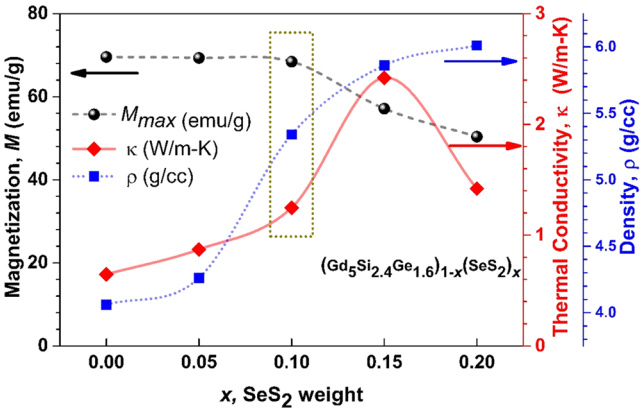

Figure 5. Comparative plot of magnetization (M_{max}), thermal conductivity, and density as a function of the SeS_2 weight amount mixed with the $Gd_5Si_{2.4}Ge_{1.6}$ alloy.

physical quantities measured at room temperature (i.e., 300 K), i.e., magnetization (M), thermal conductivity (κ), and density (ρ) as a function of the SeS_2 weight percentage. The values of magnetization shown in Figure 5 are reported at an applied magnetic field of 2 T and a temperature of 300 K. By looking at the variation in M, κ, and ρ, it can be concluded that the optimized composition to achieve the best TM properties is $(Gd_5Si_{2.4}Ge_{1.6})_{0.9}(SeS_2)_{0.1}$. This can be attributed to preserving the large magnetization along with significant improvement in the density and thermal conductivity in $(Gd_5Si_{2.4}Ge_{1.6})_{0.9}(SeS_2)_{0.1}$. A similar selection strategy has been previously reported by comparing the TM properties of Gd and La−Fe−Co−Si compounds elsewhere.[56,57] The material with a symmetrical shape of the $M-H$ curve is more suitable for magnetization and demagnetization during the TM cycle.[56]

A material with a sharp $M-H$ curve with improved ΔM is considered a good candidate for TM application. Therefore, $(Gd_5Si_{2.4}Ge_{1.6})_{0.9}(SeS_2)_{0.1}$, with a large change in magnetization and magnetic phase transition near room temperature, shows potential to be used for TM applications. We prepared SPS pellets with two different diameters (12.7 and 50 mm) and achieved similar density and thermal conductivity (Figure S5, Supporting Information). The magnetization data of samples from two different batches prepared with different diameter sizes of pellets (12.7 and 50 mm diameter) is shown in Figure S6. The MH curves of two independent batches of samples with composition $(Gd_5Si_{2.4}Ge_{1.6})_{0.9}(SeS_2)_{0.1}$ have the same magnitude and similar shape, confirming the reproducibility with the scalable point of view of making samples having different dimensions. This confirms that our approach can be upscaled without losing the material's performance.

CONCLUSIONS

We have developed a high-performance thermomagnetic alloy of $(Gd_5Si_{2.4}Ge_{1.6})_{0.9}(SeS_2)_{0.1}$ using a two-step synthesis technique: (i) induction melting was initially applied to synthesize the $Gd_5Si_{2.4}Ge_{1.6}$ ingot and (ii) the melt ingot is pulverized into a fine powder, SeS_2 is added as a sintering aid, and then the mixture is densified with low-temperature spark plasma sintering (SPS). This composite alloy shows a Curie temperature of ∼306 K. The large change in the magnetic moment within the vicinity of phase transition is preserved, while density and thermal conductivity are significantly improved by adding a small amount of SeS_2 as a sintering aid in the Gd−Si−Ge alloy. While the sintering of the Gd−Si−Ge alloy is challenging even at high temperatures, the low-temperature sintering aid is found to be very effective in processing the materials into desired shapes like pellets and rings. Microscopic analysis suggests that SeS_2 is distributed at the grain boundaries of the Gd−Si−Ge alloy, which is a key solution in strengthening the mechanical properties and achieving high density. The optimized composite materials $(Gd_5Si_{2.4}Ge_{1.6})_{0.9}(SeS_2)_{0.1}$ show a high magnetic performance of M_{max} ∼ 67 emu/g and a simultaneous large thermal conductivity of 1.25 W/m-K at 300 K and a density of 5.34 g/cm^3 in the FM state. Our study proposes that $(Gd_5Si_{2.4}Ge_{1.6})_{0.9}(SeS_2)_{0.1}$ can be a suitable composite material for low-grade waste heat recovery in thermomagnetic applications.

ASSOCIATED CONTENT

Supporting Information

The Supporting Information is available free of charge at https://pubs.acs.org/doi/10.1021/acsami.3c03158.

SEM image and EDS mapping of $(Gd_5Si_{2.4}Ge_{1.6})_{0.9}(SeS_2)_{0.1}$; temperature-dependent specific heat and temperature-dependent thermal diffusivity of $(Gd_5Si_{2.4}Ge_{1.6})_{1-x}(SeS_2)_x$ (x = 0.05, 0.1, 0.15, and 0.2); variation in thermal conductivity corresponding to the 300 K (FM) and 320 K, 360 K (PM) temperature; variation in the magnetization values, i.e., M_{max} (at 2 T) for both ferromagnetic phase (300 K) and paramagnetic phase (360 K) along with the difference $M_{max,300\ K} - M_{max,360\ K}$ as a function of SeS_2, x weight amount in $(Gd_5Si_{2.4}Ge_{1.6})_{1-x}(SeS_2)_x$ (x = 0, 0.05, 0.1, 0.15, 0.2); ingot of $Gd_5Si_{2.4}Ge_{1.6}$ obtained after induction melting; SPS pellets of $(Gd_5Si_{2.4}Ge_{1.6})_{0.9}(SeS_2)_{0.1}$ having diameters of 12.7 and 50 mm; measured density of two pellets having different diameters of 12.7 and 50 mm; measured thermal conductivity of the two pellets prepared with SPS with different diameters; and magnetization curve of the two pellets prepared with SPS with different diameters, i.e., 12.7 and 50 mm (PDF)

AUTHOR INFORMATION

Corresponding Authors

Saurabh Singh − *Department of Materials Science and Engineering, Pennsylvania State University, University Park, Pennsylvania 16802, United States;* orcid.org/0000-0003-2209-5269; Email: sbs6760@psu.edu

Amin Nozariasbmarz − *Department of Materials Science and Engineering, Pennsylvania State University, University Park, Pennsylvania 16802, United States;* orcid.org/0000-0003-2789-9469; Email: aln192@psu.edu

Bed Poudel − *Department of Materials Science and Engineering, Pennsylvania State University, University Park, Pennsylvania 16802, United States;* orcid.org/0000-0001-7760-2016; Email: bup346@psu.edu

Authors

Na Liu − *Department of Materials Science and Engineering, Pennsylvania State University, University Park, Pennsylvania 16802, United States*

Yu Zhang − *Department of Materials Science and Engineering, Pennsylvania State University, University Park, Pennsylvania 16802, United States*

Sumanta Kumar Karan − *Department of Materials Science and Engineering, Pennsylvania State University, University Park, Pennsylvania 16802, United States;* orcid.org/0000-0002-3272-3946

Lavanya Raman − *Department of Materials Science and Engineering, Pennsylvania State University, University Park, Pennsylvania 16802, United States*

Gagan Kumar Goyal − *Department of Materials Science and Engineering, Pennsylvania State University, University Park, Pennsylvania 16802, United States*

Shweta Sharma − *Department of Materials Science and Engineering, Pennsylvania State University, University Park, Pennsylvania 16802, United States;* orcid.org/0000-0002-3698-6663

Wenjie Li − *Department of Materials Science and Engineering, Pennsylvania State University, University Park, Pennsylvania 16802, United States;* orcid.org/0000-0003-4509-3303

Shashank Priya − *Department of Materials Science and Engineering, Pennsylvania State University, University Park, Pennsylvania 16802, United States*

Complete contact information is available at: https://pubs.acs.org/10.1021/acsami.3c03158

Author Contributions

The author S.S. led this work with conceptualization, data curation, formal analysis, investigation, validation, visualization, writing the original draft, review, and editing. The authors B.P., A.N., and S.P. made contributions to idea development, conceptualization, data curation, resources, and revising and reviewing the manuscript draft. The authors B.P. and S.P. played the main roles in supervision, project administration, scientific guidance, and funding acquisition. The authors N.L., Y.Z., S.K.K., L.R., G.K.G., S.S., and W.L. contributed to data curation and revising the manuscript draft.

Notes

The authors declare no competing financial interest.

ACKNOWLEDGMENTS

S.S., A.N., B.P., and S.P. acknowledge the primary financial support from the Army Research Office through the TE3 program (W911NF1620010), which is mainly responsible for this work. Auxiliary contributions of coauthors are of wide scope, spanning from material preparation, device fabrication, and a wide scope of characterizations (detailed in the Author Contribution section). The acknowledgments on these secondary supports include N.L. and G.K.G. who acknowledge the support from the Army SBIR program supported by NextGen Aeronautics, Inc. S.K.K. and W.L. acknowledge the financial support from the Army RIF program. Y.Z. acknowledges the support from the Army SBIR program supported by NanoOhmics. L.R. acknowledges support from ARPA-E through the ULTERA program. S.S. acknowledges the financial support from the National Science Foundation through the I/UCRC Program.

REFERENCES

(1) Ryu, H.; Yoon, H. J.; Kim, S. W. Hybrid energy harvesters: toward sustainable energy harvesting. *Adv. Mater.* **2019**, *31* (34), No. 1802898.

(2) Singh, S.; Hirata, K.; Pandey, S. K.; Takeuchi, T. Recent Advances in Energy Harvesting from Waste Heat Using Emergent Thermoelectric Materials. *Emerging Mater.* **2022**, 155−184.

(3) Kishore, R. A.; Priya, S. A. review on low-grade thermal energy harvesting: Materials, methods and devices. *Materials* **2018**, *11* (8), 1433.

(4) Van Vuuren, D. P.; Bijl, D. L.; Bogaart, P.; Stehfest, E.; Biemans, H.; Dekker, S. C.; Doelman, J. C.; Gernaat, D. E.; Harmsen, M. Integrated scenarios to support analysis of the food−energy−water nexus. *Nat. Sustainability* **2019**, *2* (12), 1132−1141.

(5) Forman, C.; Muritala, I. K.; Pardemann, R.; Meyer, B. Estimating the global waste heat potential. *Renewable Sustainable Energy Rev.* **2016**, *57*, 1568−1579.

(6) Schierning, G. Bring on the heat. *Nat. Energy* **2018**, *3* (2), 92−93.

(7) Kitanovski, A. Energy applications of magnetocaloric materials. *Adv. Energy Mater.* **2020**, *10* (10), No. 1903741.

(8) Dzekan, D.; Waske, A.; Nielsch, K.; Fähler, S. Efficient and affordable thermomagnetic materials for harvesting low grade waste heat. *APL Mater.* **2021**, *9* (1), No. 011105.

(9) Edison, T. A. Pyromagnetic motor. U.S. patent US380100A (Mar. 27 1888).

(10) Edison, T. A. Pyromagnetic generator, U.S. patent US476983A (June 14 1892).

(11) Srivastava, V.; Song, Y.; Bhatti, K.; James, R. D. The direct conversion of heat to electricity using multiferroic alloys. *Adv. Energy Mater.* **2011**, *1* (1), 97−104.

(12) Kishore, R. A.; Priya, S. A review on design and performance of thermomagnetic devices. *Renewable Sustainable Energy Rev.* **2018**, *81*, 33−44.

(13) Chun, J.; Song, H. C.; Kang, M. G.; Kang, H. B.; Kishore, R. A.; Priya, S. Thermo-magneto-electric generator arrays for active heat recovery system. *Sci. Rep.* **2017**, *7* (1), No. 41383.

(14) Bozorth, R. *Ferromagnetism*; Wiley: Hoboken, NJ, 1993.

(15) Bjørk, R.; Bahl, C. R. H.; Katter, M. Magnetocaloric properties of $LaFe_{13-x-y}Co_xSi_y$ and commercial grade Gd. *J. Magn. Magn. Mater.* **2010**, *322* (24), 3882−3888.

(16) Hu, F. X.; Gao, J.; Qian, X. L.; Ilyn, M.; Tishin, A. M.; Sun, J. R.; Shen, B. G. Magnetocaloric effect in itinerant electron metamagnetic systems $La(Fe_{1-x}Co_x)_{11.9}Si_{1.1}$. *J. Appl. Phys.* **2005**, *97* (10), No. 10M303.

(17) Lin, S.; Wang, B. S.; Lin, J. C.; Zhang, L.; Hu, X. B.; Huang, Y. N.; Lu, W. J.; Zhao, B. C.; Tong, P.; Song, W. H.; Sun, Y. P. Composition dependent-magnetocaloric effect and low room-temperature coefficient of resistivity study of iron-based antiperovskite compounds Sn1−xGaxCFe3 (0≤ x≤ 1.0). *Appl. Phys. Lett.* **2011**, *99* (17), No. 172503.

(18) Wang, B. S.; Tong, P.; Sun, Y. P.; Zhu, X. B.; Luo, X.; Li, G.; Song, W. H.; Yang, Z. R.; Dai, J. M. Reversible room-temperature magnetocaloric effect with large temperature span in antiperovskite compounds Ga 1−xCMn3+x (x= 0, 0.06, 0.07, and 0.08). *J. Appl. Phys.* **2009**, *105* (8), No. 083907.

(19) Zhong, W.; Chen, W.; Au, C. T.; Du, Y. W. Dependence of the magnetocaloric effect on oxygen stoichiometry in polycrystalline $La_{2/3}Ba_{1/3}MnO_{3-\delta}$. *J. Magn. Magn. Mater.* **2003**, *261* (1−2), 238−243.

(20) Hou, D. L.; Yue, C. X.; Bai, Y.; Liu, Q. H.; Zhao, X. Y.; Tang, G. D. Magnetocaloric effect in $La_{0.8-x}Nd_xNa_{0.2}MnO_3$. *Solid State Commun.* **2006**, *140* (9−10), 459−463.

(21) Yu, P.; Zhang, J. Z.; Xia, L. $Fe_{87}Zr_7B_4Co_2$ amorphous alloy with excellent magneto-caloric effect near room temperature. *Intermetallics* **2018**, *95*, 85−88.

(22) Wang, Z. W.; Yu, P.; Cui, Y. T.; Xia, L. Near room temperature magneto-caloric effect of a $Gd_{48}Co_{52}$ amorphous alloy. *J. Alloys Compd.* **2016**, *658*, 598−602.

(23) Dan'Kov, S. Y.; Tishin, A. M.; Pecharsky, V. K.; Gschneidner, K. A. Magnetic phase transitions and the magnetothermal properties of gadolinium. *Phys. Rev. B* **1998**, *57* (6), 3478.

(24) Meis, C.; Froment, A. K.; Moulinier, D. Determination of gadolinium thermal conductivity using experimentally measured values of thermal diffusivity. *J. Phys. D: Appl. Phys.* **1993**, *26* (4), 560.

(25) Tegus, O.; Brück, E.; Zhang, L.; Dagula; Buschow, K. H. J.; De Boer, F. R. Magnetic-phase transitions and magnetocaloric effects. *Phys. B: Condens. Matter* **2002**, *319* (1−4), 174−192.

(26) Pyykkö, P. Magically magnetic gadolinium. *Nat. Chem.* **2015**, *7* (8), 680.

(27) Kishore, R. A.; Singh, D.; Sriramdas, R.; Garcia, A. J.; Sanghadasa, M.; Priya, S. Linear thermomagnetic energy harvester for low-grade thermal energy harvesting. *J. Appl. Phys.* **2020**, *127* (4), No. 044501.

(28) Phillips, M. R.; Carman, G. P. Numerical analysis of an active thermomagnetic device for thermal energy harvesting. *J. Energy Resour. Technol.* **2020**, *142* (8), No. 082102.

(29) Chen, H.; Ma, Z.; Liu, X.; Qiao, K.; Xie, L.; Li, Z.; Shen, J.; Dai, W.; Ou, Z.; Yibole, H.; Tegus, O.; et al. Evaluation of thermomagnetic generation performance of classic magnetocaloric materials for harvesting low-grade waste heat. *Appl. Energy* **2022**, *306*, No. 117999.

(30) Dolejsi, D. A.; Swenson, C. A. Experimental thermal expansivities for single-crystal gadolinium metal near the Curie temperature. *Phys. Rev. B* **1981**, *24* (11), 6326.

(31) Seyoum, H. M.; Ghahremani, M.; ElBidweihy, H.; Bennett, L. H.; Della Torre, E. Evidence of metastability near the Curie temperature of polycrystalline gadolinium. *J. Appl. Phys.* **2012**, *112* (11), No. 113913.

(32) Ergün, Y. A. Mechanical properties of epoxy composite materials produced with different ceramic powders. *J. Mater. Sci. Chem. Eng.* **2019**, *07* (12), 1−8.

(33) Kim, H. T. High thermal conductivity ceramics and their composites for thermal management of integrated electronic packaging. In *Heat Transfer-Models, Methods and Applications*; IntechOpen, 2018; pp 333−359.

(34) Spichkin, Y. I.; Pecharsky, V. K.; Gschneidner, K. A. Preparation, crystal structure, magnetic and magnetothermal properties of $(Gd_xR_{5-x})Si_4$, where R= Pr and Tb, alloys. *J. Appl. Phys.* **2001**, *89* (3), 1738−1745.

(35) Holtzberg, F.; Gambino, R. J.; McGuire, T. R. New ferromagnetic 5:4 compounds in the rare earth silicon and germanium systems. *J. Phys. Chem. Solids* **1967**, *28* (11), 2283−2289.

(36) Gschneidner, K. A., Jr.; Pecharsky, V. K.; Pecharsky, A. O.; Zimm, C. B. Recent developments in magnetic refrigeration. In *Materials Science Forum*; Trans Tech Publications Ltd., 1999; Vol. *315*, pp 69−76.

(37) Elbicki, J. M.; Zhang, L. Y.; Obermyer, R. T.; Wallace, W. E.; Sankar, S. G. Magnetic studies of $(Gd_{1-x}M_x)_5Si_4$ alloys (M= La or Y). *J. Appl. Phys.* **1991**, *69* (8), 5571−5573.

(38) Pecharsky, V. K.; Gschneidner, K. A., Jr Giant magnetocaloric effect in $Gd_5(Si_2Ge_2)$. *Phys. Rev. Lett.* **1997**, *78* (23), 4494.

(39) Pecharsky, A. O.; Gschneidner, K. A., Jr; Pecharsky, V. K.; Schindler, C. E. The room temperature metastable/stable phase relationships in the pseudo-binary Gd_5Si_4−Gd_5Ge_4 system. *J. Alloys Compd.* **2002**, *338* (1−2), 126−135.

(40) Gębara, P.; Díaz-García, Á.; Law, J. Y.; Franco, V. Magnetocaloric response of binary Gd-Pd and ternary Gd-(Mn, Pd) alloys. *J. Magn. Magn. Mater.* **2020**, *500*, No. 166175.

(41) Díaz-García, Á.; Law, J. Y.; Gębara, P.; Franco, V. Phase deconvolution of multiphasic materials by the universal scaling of the magnetocaloric effect. *JOM* **2020**, *72* (8), 2845−2852.

(42) Law, J. Y.; Moreno-Ramírez, L. M.; Blázquez, J. S.; Franco, V.; Conde, A. Gd+ GdZn biphasic magnetic composites synthesized in a single preparation step: Increasing refrigerant capacity without decreasing magnetic entropy change. *J. Alloys Compd.* **2016**, *675*, 244−247.

(43) Gębara, P.; Hasiak, M. Determination of phase transition and critical behavior of the as-cast GdGeSi-(x) type alloys (where x= Ni, Nd and Pr). *Materials* **2021**, *14* (1), 185.

(44) Mishra, R.Synthesis of Materials by Induction Heating. In *Handbook on Synthesis Strategies for Advanced Materials: Volume-I: Techniques and Fundamentals*; Springer: Singapore, 2021; pp 215−228. DOI: 10.1007/978-981-16-1807-9_8.

(45) Serdyuk, U. V.; Krentsis, R. P.; Geld, P. V. Interrelation of specific heat and electrical resistivity in rare earth silicides R_5Si_4. *J. Less-Common Met.* **1985**, *111* (1−2), 347−352.

(46) Zeng, H.; Zhang, J.; Kuang, C. In-situ reaction synthesis of pure bulk gadolinium dihydride materials. *Intermetallics* **2010**, *18* (3), 369−373.

(47) Samudrala, G. K.; Tsoi, G. M.; Weir, S. T.; Vohra, Y. K. Structural and magnetic phase transitions in gadolinium under high pressures and low temperatures. *High Pressure Res.* **2014**, *34* (4), 385−391.

(48) Vijayan, P. P. Spectroscopy and X-ray Scattering Studies of Epoxy Composites. *Epoxy Compos.* **2021**, 217−240.

(49) Premchander, P.; Baskar, K.; Jayavel, R.; Arivuoli, D.; Palanichamy, M. Growth and characterization of selenium sulfide (SeS) and selenium tin sulfide ($SeSnS_2$) microcrystals. *J. Cryst. Growth* **2004**, *263* (1−4), 498−503.

(50) Hirata, K.; Matsunaga, T.; Saurabh, S.; Matsunami, M.; Takeuchi, T. Development of high-performance solid-state thermal diodes using unusual behavior of thermal conductivity observed for Ag_2Ch (Ch= S, Se, Te). *MATER. TRANS.* **2020**, *61* (12), 2402−2406.

(51) Byeon, D.; Sobota, R.; Hirata, K.; Singh, S.; Choi, S.; Adachi, M.; Yamamoto, Y.; Matsunami, M.; Takeuchi, T. Dynamical variation of carrier concentration and colossal Seebeck effect in Cu_2S low-temperature phase. *J. Alloys Compd.* **2020**, *826*, No. 154155.

(52) Singh, S.; Hirata, K.; Byeon, D.; Matsunaga, T.; Muthusamy, O.; Ghodke, S.; Adachi, M.; Yamamoto, Y.; Matsunami, M.; Takeuchi, T. Investigation of Thermoelectric Properties of Ag 2 S x Se 1− x (x= 0.0, 0.2 and 0.4). *J. Electron. Mater.* **2020**, *49*, 2846−2854.

(53) Li, X.; Kim, M.; Zhai, W. Ceramic microlattice and epoxy interpenetrating phase composites with simultaneous high specific strength and specific energy absorption. *Mater. Des.* **2022**, *223*, No. 111206.

(54) Olhero, S. M.; Lopes, E.; Ferreira, J. M. F. Fabrication of ceramic microneedles−The role of specific interactions between processing additives and the surface of oxide particles in Epoxy Gel Casting. *J. Eur. Ceram. Soc.* **2016**, *36* (16), 4131−4140.

(55) Kishore, R. A.; Davis, B.; Greathouse, J.; Hannon, A.; Kennedy, D. E.; Millar, A.; Mittel, D.; Nozariasbmarz, A.; Kang, M. G.; Kang, H. B.; Sanghadasa, M.; Priya, S. Energy scavenging from ultra-low temperature gradients. *Energy Environ. Sci.* **2019**, *12* (3), 1008−1018.

(56) Dzekan, D.; Diestel, A.; Berger, D.; Nielsch, K.; Fähler, S. Can gadolinium compete with La-Fe-Co-Si in a thermomagnetic generator? *Sci. Technol. Adv. Mater.* **2021**, *22* (1), 643−657.

(57) Waske, A.; Dzekan, D.; Sellschopp, K.; Berger, D.; Stork, A.; Nielsch, K.; Fähler, S. Energy harvesting near room temperature using

a thermomagnetic generator with a pretzel-like magnetic flux topology. *Nat. Energy* **2019**, *4* (1), 68−74.
(58) Cotton, S. *Lanthanide and Actinide Chemistry*; John Wiley & Sons, 2013.
(59) Yost, D. M.; Russell, H., Jr.; Garner, C. S. *The Rare-Earth Elements and their Compounds*; Wiley, 1947.

https://doi.org/10.1021/acsami.3c03158
ACS Appl. Mater. Interfaces XXXX, XXX, XXX−XXX